ISSN 0016-7932, Geomagnetism and Aeronomy, 2021, Vol. 61, No. 2, pp. 277–286. © Pleiades Publishing, Ltd., 2021.

Statistical Analysis of Storm-time TEC Variation during Ascending and Descending Solar Periods of 24th Solar Cycle

Erman Şentürk*

Kocaeli University, Department of Geomatics Engineering, Kocaeli, Turkey

**e-mail: erman.senturk@kocaeli.edu.tr*

Received July 3, 2019; revised July 14, 2020; accepted September 24, 2020

Abstract– This paper presents a statistical analysis of global ionospheric variation during quiet and disturbed geomagnetic conditions from December 2008 to June 2019. The study comprehends ascending and descending solar periods of the 24th solar cycle. The vertical Total Electron Content (vTEC) data of CODE-GIM are utilized to reveal the TEC variation in the regional and global regions. The disturbance storm time index (*Dst*) with a storm criterion of diurnal Dst_{min} less than −20 nT was used to identify the magnetically quiet/disturbed conditions, and the geomagnetic storms were identified by diurnal Dst_{min} less than −50 nT. 36 and 43% of the ascending/descending periods were magnetically disturbed days, respectively. There was no significant change in vTEC variation in the high and middle latitude regions. Still, in the low latitudes, vTECs increased 50 and 25% in the disturbed days of ascending/descending periods, respectively. vTEC values in the low latitudes were found to be 33% higher than the middle latitudes and 100% higher than the high latitudes in quiet days for both periods. vTEC values in the low latitudes were also found to be 50 and 200% higher than the middle and high latitudes in disturbed days, respectively. Also, the Dst and global Total Electron Content (gTEC) variations were compared using the superposed epoch analysis (SEA) for geomagnetic storms. The gTEC values indicate the average vTEC of CODE-GIM grids. The SEA results indicate that the gTEC variation is similar to the Dst pattern of a magnetic storm. The mean gTEC values decreased shortly after when the storm was peaked, corresponding to approximately 20 and 17% in ascending and descending periods, respectively.

DOI: 10.1134/S0016793221020146

INTRODUCTION

The ionosphere is a non-uniform and anisotropic atmosphere layer ranging between 80 and 1500 km from the earth's surface. This layer contains gases that form the ionized plasma by changing its state due to solar radiation. The ions and electrons are formed as a pair due to ionization. Free and mobile electrons affect electromagnetic signals depending on their frequencies. The ionospheric variation is influenced by space weather events such as solar winds, solar flares, geomagnetic storms. The disturbed space weather conditions trigger unexpected irregular changes in the magnetosphere-ionosphere-thermosphere system.

A magnetic storm is caused by a solar flare or coronal mass ejection (CME) (de Abreu et al., 2017) and has three phases; initial, main, and recovery. The interplanetary magnetic field carried by the solar winds induces the deformation of the earth's magnetic field bumping into the magnetosphere. The degree of strain is related to the speed and density of the solar winds. Patel et al. (2019) mentioned that CMEs are the primary source of geomagnetic storms. The geomagnetic/ionospheric storms cause significant positive and negative phases in the ionosphere, which depend on the onset time of the storm, season, solar activity level, and the location (Prölss, 1995).

The different mechanisms of the ionospheric response tried to be explained with various assumptions. Prölss (1995) described negative ionospheric storms with the changes in the neutral gas composition. The depletion of electron density during negative ionospheric storms is well correlated with the decrease in the O/N_2 ratio (Habarulema et al., 2013; Katamzi and Habarulema, 2014). Also, ionospheric disturbance dynamo is a factor to produce negative ionospheric storm effects (Blanc and Richmond, 1980).

On the other hand, it is believed that the prompt penetration electric field causes positive ionospheric storms due to uplifting plasma to higher altitudes in the equatorial and mid-latitude ionosphere. As altitude increases, air density decreases; thus, the recombination rate of ions and electrons is lower. Also, the uplifting plasma in the equatorial ionosphere spreads along geomagnetic field lines and causes the propagation of the equatorial ionization anomaly toward mid-latitudes (Gonzalez et al., 2005). The other co-decision mechanism of positive ionospheric storms is, traveling through the atmospheric disturbances. This

phenomenon is generated by meridional winds carrying along equatorward directed, which causes the enhancement of electron density in the middle latitudes (Bauske and Prölss, 1997). Rees (1995) reviewed the chemical, dynamical and electro-dynamical interactions between the thermosphere and ionosphere during intense geomagnetic storms. The study revealed that the ionospheric variation is not only affected by changes in ionization sources and electric fields but also simultaneous changes of density, composition, and flows of the thermosphere. Buonsanto (1999) reviewed the ionospheric storm effects on thermosphere, D, E, and F layers of the ionosphere at high, middle, and low latitudes. The F2 layer response to geomagnetic storms during the storm and pre-storm periods also discussed extensively by Danilov (2013) and Danilov and Konstantinova (2019).

Some case studies related to storm-time ionospheric response in a global and regional manner were published for several intense storms (e.g., Batista et al., 1991; Ding et al., 2007; Grigorenko et al., 2007; Khegai et al., 2009; Inyurt, 2020; Şentürk, 2020). Many researchers also conducted the statistical studies (e.g., Liu et al., 2005; Kumar et al., 2006; Dmitriev et al., 2013; Matamba et al., 2015; Yang et al., 2016; Timoçin, 2019). Liu et al. (2005) examined the ratio of N+/O+ in the current ring region. They found the rate of N+/O+ as about 0.314 during quiet times. The statistical results showed a decrease in the ratio of N+/O+ for intense storms, whereas there is no apparent correlation for small storms. Kumar et al. (2006) investigated 102 magnetic storms with different intense between 1997 and 2001. They found that 35% of magnetic storms were associated with magnetic clouds. The storm-time F2-region response of Ahmedabad (23.2° N, 72.4° E) station is also studied for 51 magnetic storms. The results showed more distinct negative ionospheric effects than positive ones. They indicated that the prompt penetration of high-latitude electric fields and the disturbance dynamo play an essential role in F2-region response by altering E × B drifts at low latitude. Also, the decrease in the ratio of O/N_2 may be the primary driver of the post-midnight significant decline in foF2, during intense magnetic storms ($Dst < 100$ nT). Dmitriev et al. (2013) analyzed the positive ionospheric storms in the dayside region of the equatorial ionization anomaly during recurrent geomagnetic storms from 2004 to 2008. The vertical profiles of electron content showed that the F2 layer thickens, NmF2 increases by similar to 50%, and hmF2 elevated by a few tens of kilometers in peak intensity of an ionospheric storm on March 28, 2008. The response of positive ionospheric storms reveals an evident longitudinal asymmetry. Increases in TECs have the highest correlations with the heliospheric and geomagnetic drivers in December and February. Matamba et al. (2015) done a statistical analysis of ionospheric response over South Africa with the foF2 and TEC data during the period 1996–2011. The results showed a strong solar cycle dependence with negative/positive phases. The percentage of phases in the seasons were determined as 63.24% in summer and 53.62% in winter. Yang et al. (2016) investigated the variations of mid-latitude statistically troughs in 129 moderate and intense magnetic storms in the 23rd solar cycle. The results showed that the trough moves toward the equator/pole during the Dst index decreases/increases. They found a strong correlation between the minimum latitude of the trough position and the storm magnitude. Timoçin (2019) studied the effect of severe geomagnetic storms during 1981 and 1991 with hourly foF2 data measured at the low latitude ionosonde station Manila. The results showed that the foF2 values increase in the daytime while decrease at nighttime during the main phase. The foF2 values also decrease at day hours, while increase at night hours during the recovery phase. Also, the changes in the foF2 values in the recovery phase are more significant than the main phase. In the present study, some statistical results of storm-time TEC variation during magnetic storms of the 24th solar cycle were introduced for the global and regional ionosphere.

DATA AND ANALYSIS

A time period from December 1, 2008 (DOY: 336) to June 30, 2019 (DOY : 181) was selected to perform a statistical analysis of magnetic storms and storm/quiet time TEC response in the 24th solar cycle. Figure 1a shows the monthly sunspot numbers (R) and its smoothed values by the weighted linear least-squares method. A solar cycle has two periods: ascending and descending. The monthly R values show that the descending period of the 24th solar cycle started after February 7, 2014 (DOY : 38). It is observed that smoothed R values peaked between 2011 and 2012 during the ascending period. R values should be about 60, while it suddenly increases up to 130. This sudden increase in the 2nd six months of 2011 caused to three intense magnetic storms (-100 nT $> Dst > -200$ nT). 1st six months of 2011 have no intense or super ($Dst < -200$ nT) magnetic storm (see Fig. 1b). The descending period moved more linearly than the ascending period. Only in the first quarter of 2015, there was a sharp decrease and then a sudden increase in R values. During this period, two super storms occurred on March 17, 2015, with an hourly Dst_{min} value of -223 nT and June 22, 2015, with an hourly Dst_{min} value of -204 nT.

In Figure 2 and Table 1, yearly quiet days (QD) and disturbed days (DD) of the 24th solar cycle were shown. QD and DD are determined by considering diurnal Dst_{min} values with a threshold value of -20 nT. If the daily Dst_{min} value is less than -20 nT, the relevant day is accepted as DD. It was determined that 36% of the ascending period and 43% of the descending period were DD. The highest DD count of the ascending period is in the year of 2012, and the highest

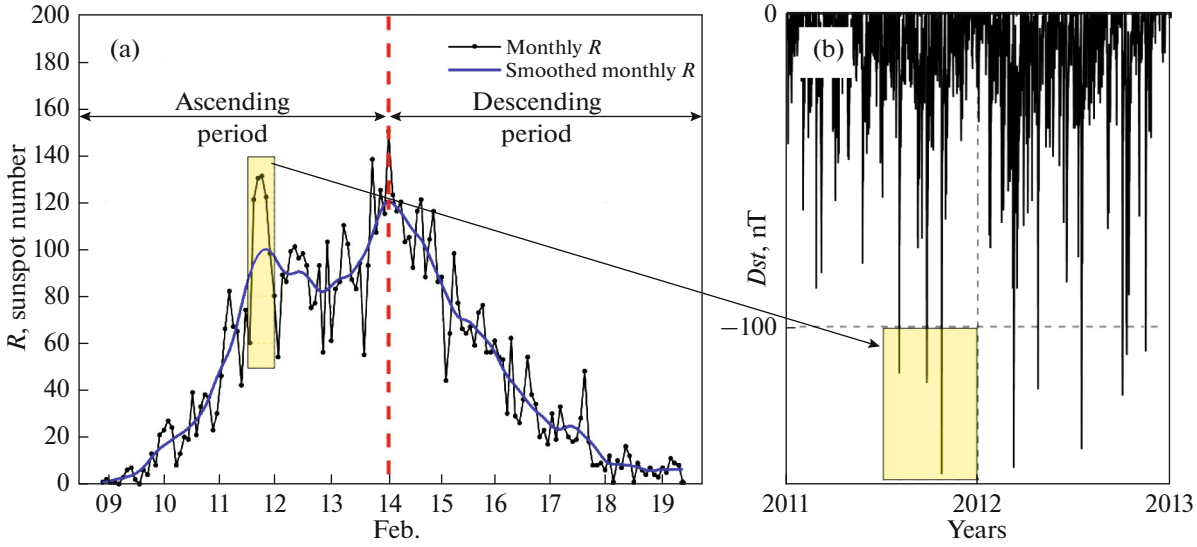

Fig. 1. Monthly *R*, smoothed monthly *R* (a) and *Dst* values (b) from December 1, 2008 to June 30, 2019.

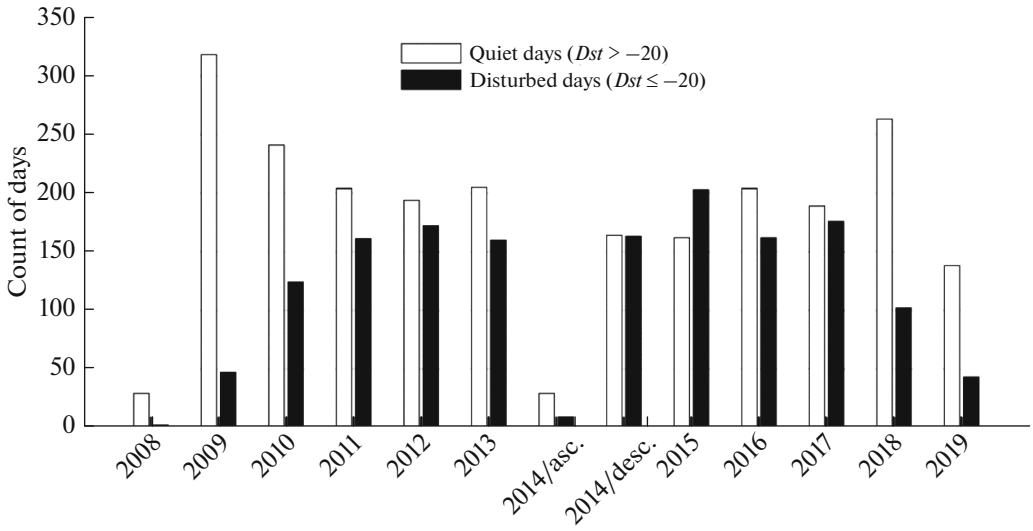

Fig. 2. Yearly QD and DD of 24th solar cycle.

DD of the descending period is in the year of 2015. Only in 2015, DD is more than QD. The count of DD in the relevant year has been determined as 56%.

Fifteen intense storms occurred in the ascending period, while eleven intense and two super storms occurred in the descending period. The pattern of monthly *R* values and the count of DD similar to the normal distribution curve by years. There is a high degree of positive correlation between the monthly *R* and count of DD.

The global Total Electron Content (gTEC) values were utilized to analyze storm-time global TEC response in ascending/descending periods of the 24th solar cycle. The gTEC is calculated by,

$$\mathrm{gTEC} = \frac{\sum_{i}^{m}\sum_{j}^{n} \mathrm{vTEC}_{i,j}}{mn}, \quad (1)$$

where *m* and *n* are the number of grids along latitudes and longitudes. *i* and *j* start from 1.

The SEA is a statistical approach applied to time series and utilized for the statistical comparison of different space weather and atmospheric/ionospheric data (Taylor et al., 1994; Davis et al., 1997; Ilie et al., 2008; Katus et al., 2015; Timoçin, 2019; Yin et al., 2019). The superposed epoch analysis was applied to introduce common and different variations of Dst and

Table 1. Statistics of yearly QD and DD

Solar activity status	Total QD	Total DD	Year	$Dst > -20$	$-50 \le Dst \le -20$	$-100 \le Dst < -50$	$-200 \le Dst < -100$	$Dst < -200$
Ascending	1220	675	2008[1]	29	2	0	0	0
			2009	318	46	1	0	0
			2010	241	108	16	0	0
			2011	204	133	24	4	0
			2012	194	127	37	8	0
			2013	205	127	30	3	0
			2014[2]	29	9	0	0	0
Descending	1120	849	2014[3]	164	135	27	1	0
			2015	162	151	45	5	2
			2016	204	131	29	2	0
			2017	189	159	15	2	0
			2018	263	95	6	1	0
			2019[4]	138	41	2	0	0

[1] Day of the year from 336 to 366 in the year of 2008 [2] Day of the year from 001 to 038 in the year of 2014 [3] Day of the year from 039 to 365 in the year of 2014 [4] Day of the year from 001 to 181 in the year of 2019.

gTEC data. This comparison contributes to understanding the storm-time responses of global TEC.

RESULTS

Global TEC Variation

The diurnal mean vTEC of CODG-GIMs were analyzed to investigate global TEC variation during QD and DD. Figure 3 shows the average vTEC maps of the QD and DD in the ascending period and their standard deviations. Global TEC variation was obtained by averaging diurnal vTEC maps of 1220 QD and 675 DD. Figure 3 demonstrated that there was no significant change in vTEC variation in the high and middle latitude regions. However, it was determined that there was a 50% increase in vTECs and standard deviations of DDs relative to QDs in the low latitude region. Figures 3d, 3h indicated that the average F10.7 values in the QD are 97.5 sfu, and the average F10.7 values in the DD are 109.9 sfu.

Figure 4 shows the average vTEC maps of the QD and DD in the descending period and their standard deviations. Global TEC variation was obtained by averaging diurnal vTEC maps of 1120 QD and 849 DD. There was no significant change in vTEC variation in the high and middle latitude regions, but, there was a 25% increase in vTECs and a 33% increase in standard deviations of DDs relative to QDs in the low latitude region. Figures 3d, 3h indicated that the average F10.7 values in the QD are 91.1 sfu, and the average F10.7 values in the DD are 102.7 sfu. It is determined that the average F10.7 values in the ascending period are 7% higher than in the descending period.

Both ascending and descending periods, vTEC values in the low latitudes were found to be 33% higher than the middle latitudes and 100% higher than the high latitudes in QDs. Also, vTEC values in the low latitudes were found to be 50% higher than the middle latitudes and 200% higher than the high latitudes in DDs. Figures 3 and 4 show the distinction between low, middle, and high latitude regions, considering the variation of vTEC values. Dark blue areas depict the high latitude region (between 90° and 50° of hemispheres), while light blue and turquoise areas (between 50° and 30° of hemispheres) are the middle latitude region, and yellow, orange and brown areas (between 30° and 0° of hemispheres) depict the low latitude region.

Longitudinal TEC Variation

The average values of diurnal vTEC variation for three different sectors in QD and DD were obtained for longitudinal analysis. These sectors are America (70° W), Europe-Africa (20° E), and Asia-Australia (130° E). In Figure 5, the vertical axis shows latitudes, and the horizontal axis shows the hours of the day with a 2-hour interval.

The maximum, average, and root-mean-square error (RMSE) values of three different sectors in QD and DD of ascending/descending periods were given in Table 2. The unit of all values is TECU. Table 2 proves that the vTEC values in the ascending period are relatively higher than the descending period in both the QD and DD. It was also determined that the vTEC values in the American sector are relatively higher than in the other two sectors. 31–33% increase in the ascending/descending periods were found in

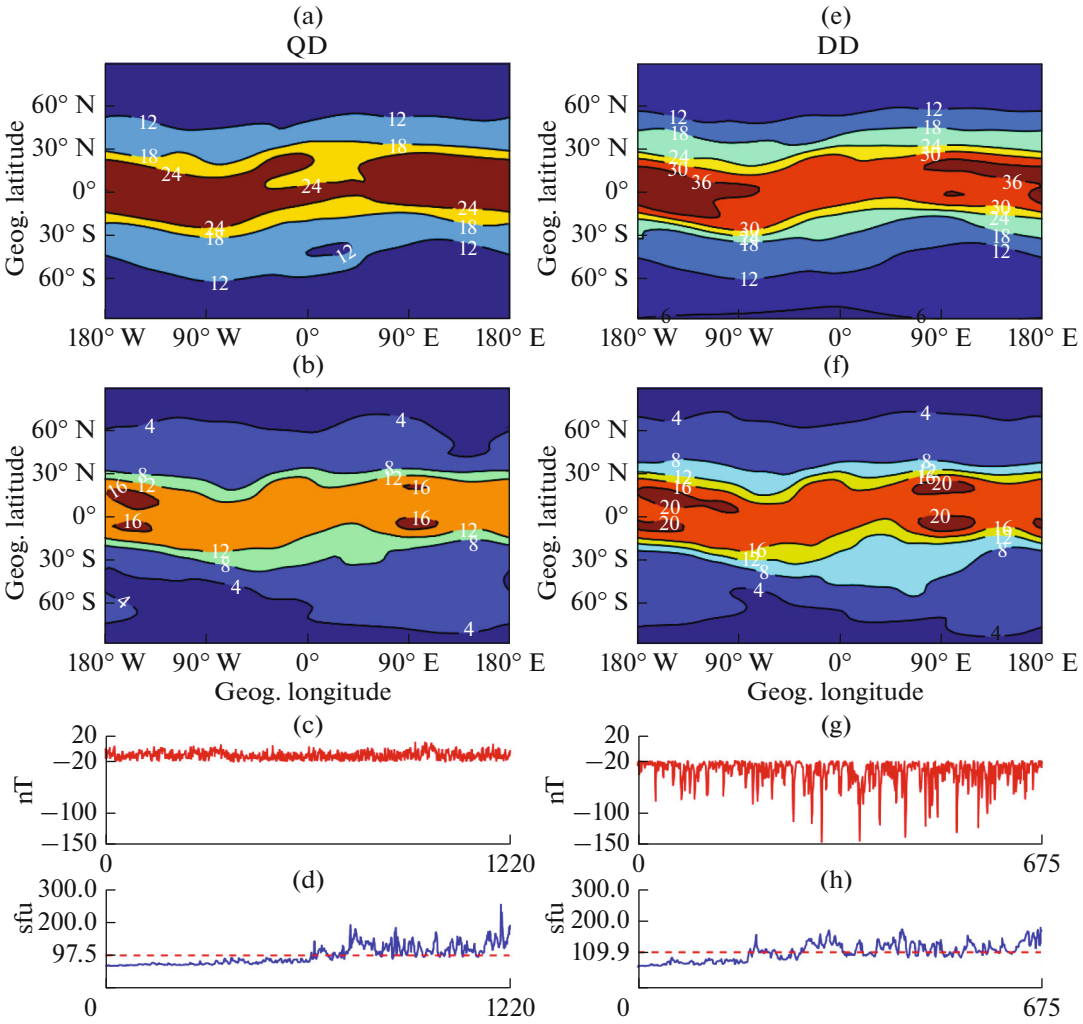

Fig. 3. Global vTEC variation in QD and DD of ascending period (a) mean vTEC of QD (b) standard deviation of vTECs in QD (c) diurnal Dst_{min} values in QD (d) F10.7 values in QD (e) mean vTEC of DD (f) standard deviation of vTECs in DD (g) diurnal Dst_{min} values in DD (h) F10.7 values in DD.

DDs for all sectors. There was a 16–19% increase in mean values during the ascending period and a 24–28% increase during the descending period. Also, there was an increase of 22–25% in the ascending period and 28–32% in the descending period in RMSE values.

Superposed Epoch Analysis

The superposed epoch analysis is a frequently used statistical method to reveal the characteristic behavior of multiple event time series. In this study, SEA was applied to the Dst and gTEC time series, including a

Table 2. Maximum, mean and RMSE values of three different sectors

Sector	Ascending						Descending					
	DD			QD			DD			QD		
	max	mean	RMSE	max	mean	RMSE	max	mean	RMSE	max	mean	RMSE
American	65.2	18.7	23.2	49.7	15.7	18.6	60.6	17.9	22.2	45.5	14.0	16.8
European-African	56.5	16.7	20.9	43.2	14.4	17.1	54.1	15.9	19.8	40.7	12.8	15.5
Asia-Australian	62.6	17.8	22.1	48.0	14.9	17.8	58.0	16.4	20.5	43.7	13.2	16.0

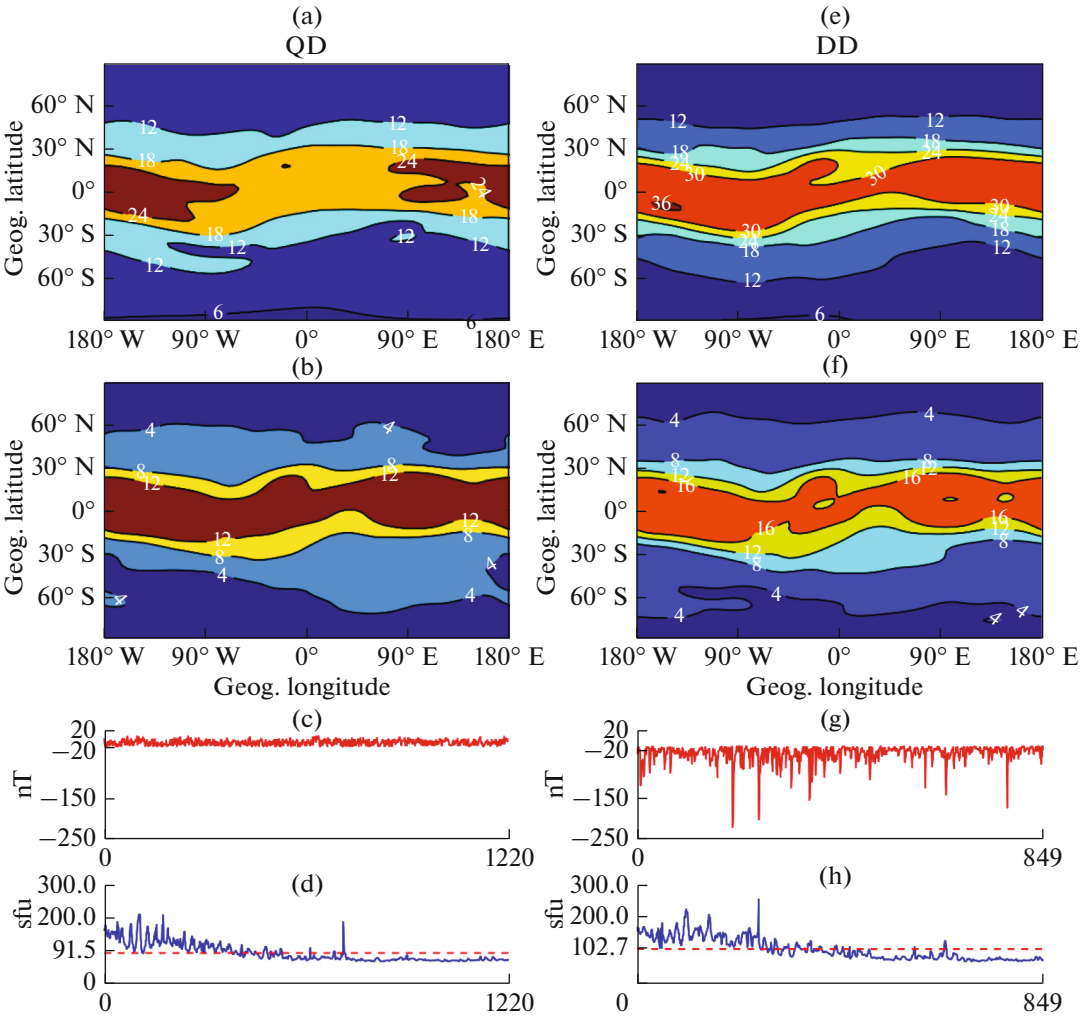

Fig. 4. Global vTEC variation in QD and DD of descending period (a) mean vTEC of QD (b) standard deviation of vTECs in QD (c) diurnal Dst_{min} values in QD (d) F10.7 values in QD (e) mean vTEC of DD (f) standard deviation of vTECs in DD (g) diurnal Dst_{min} values in DD (h) F10.7 values in DD.

5-day interval for 126 magnetic storms. The magnetic storms were manually selected according to diurnal $Dst_{min} \leq -50$ nT, in which 47% (59/126) of these storms occurred in the ascending and 53% (67/126) descending periods. The peak Dst_{min} values of events are interfaced to apply the SEA. The epoch markers start with peak times. The timelines of the series are in the 24 hours before the epoch marker and following 96 hours. The results of the SEA are shown in Figs. 6, 7. In Figures, the *y*-axis is limited as −250–100 nT for *Dst* and is defined as 0–40 TECU for gTEC. The graphs of mean gTEC are also limited from 13 to 18 TECU. These common limits were selected to examine the status of behavior in both the ascending and descending periods. The y-axis is the magnitude of the indices, and the *x*-axis is the timeline. The dashed black vertical lines define the epoch markers which define the start or end of each storm phase. The SEA was applied with bins of 1 h along the *x*-axis and 5 nT (*Dst*) and 1 TECU (gTEC) along the *y*-axis. The colors present the density of data points in each bin. The mean of Dst and gTEC along the timeline are shown in black lines of SEA plots.

Figure 6 shows the *Dst* and gTEC data density for 59 geomagnetic storms during the ascending period along the epoch timeline. The mean of *Dst* values indicates a mean peak of −80 nT for all of the storms. It was observed that Dst values ranged between −35 nT and −15 nT during the recovery phase. There is an interesting feature in the SEA of gTEC. The density and mean values of gTEC are similar to common Dst variation during a magnetic storm. The mean gTEC values have a sudden decrease after the epoch marker. The decline was approximately 20% (from 17.7 to 14 TECU) in Fig. 6c. The gTEC values are the mean of vTEC values of 5184 grids in CODE-GIMs with 2-h temporal resolution. These values are ranged between

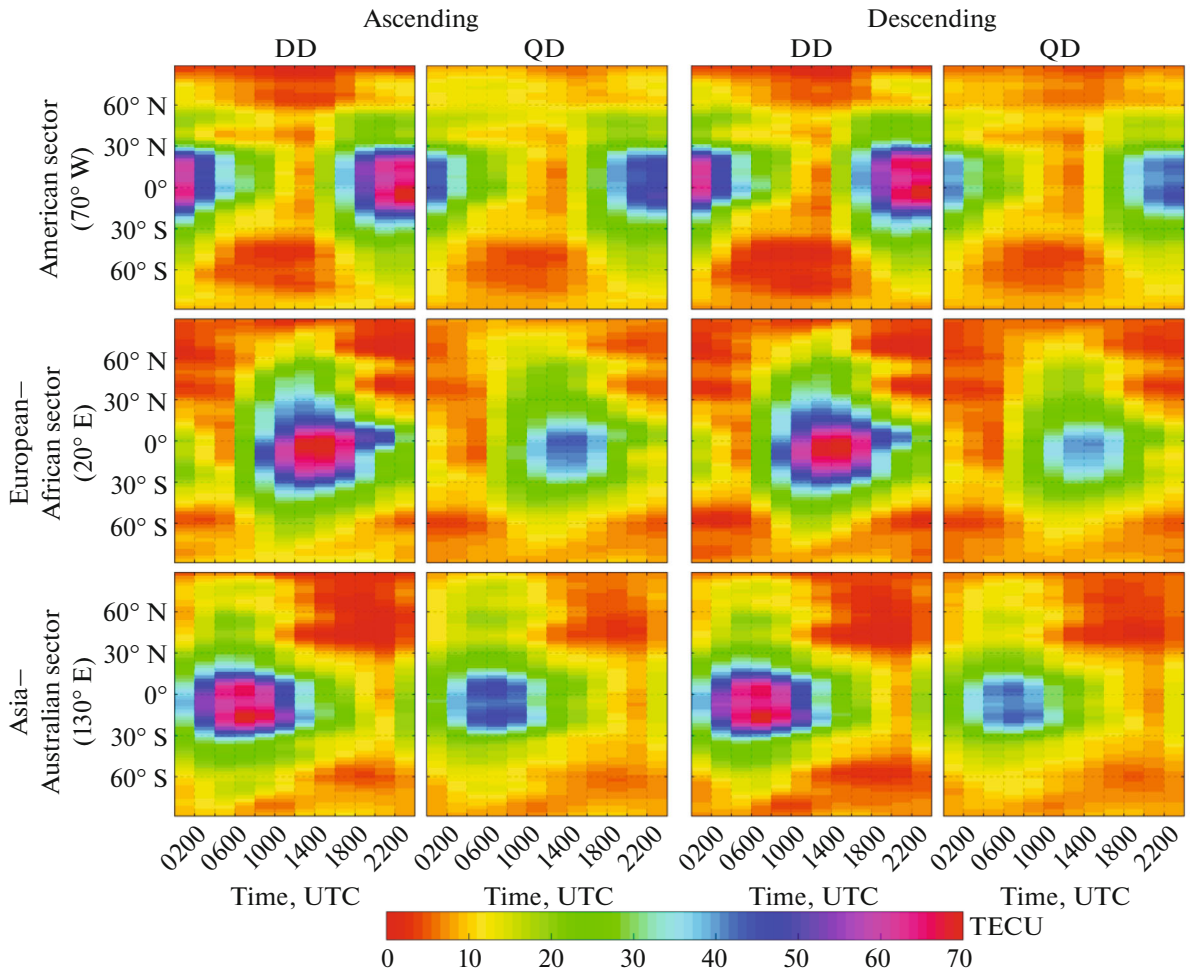

Fig. 5. Diurnal vTEC variation in three different sectors in QD and DD of ascending and descending periods.

10 TECU and 20 TECU in ascending period according to the density of data.

Figure 7 shows the Dst and gTEC data density for 67 geomagnetic storms during the descending period along the epoch timeline. The average *Dst* values indicate a peak of −80 nT for all of the storms similar to the ascending period. Dst values ranged between −35 nT and 0 nT during the recovery phase. In the descending period, the Dst values have a wider spectrum in the recovery phase in regards to the ascending period and also have a faster recovery phase because the *Dst* values reaching to 0 nT at a shorter time. The density and mean values of gTEC are similar to common *Dst* variation during a magnetic storm. The mean gTEC values have a sudden decrease after the epoch marker. The decline was approximately 17% (from 15.9 to 13.2 TECU) in Fig. 7c. The gTEC values are ranged between 5 TECU and 15 TECU according to the density of data, but the gTEC variations are wider in the descending period than the ascending period.

CONCLUSIONS

This study shows some significant differences in the TEC response originated from magnetic storms during the ascending and descending periods of the 24th solar cycle. The ascending period was defined between December 1, 2008, and February 6, 2014, and the descending period between February 7, 2014, and June 30, 2019. The ascending covers 1895 days, and 36% of them correspond to the magnetically disturbed day according to the threshold value diurnal $Dst_{min} \leq -20$ nT. The descending covers a period of 1969 day, 43% of which corresponds to the disturbed day. Although DD was more in the descending period, 15 intense storms occurred in the ascending period and 13 intense storms (two of them are super storms) in the descending period. Also, the average F10.7 values in the ascending period are 7% higher than in the descending period. It was determined that there is a high degree of the positive correlation between monthly R and DD by years.

In global, the storm-time TEC responses were analyzed within vTEC values of CODE-GIMs. The aver-

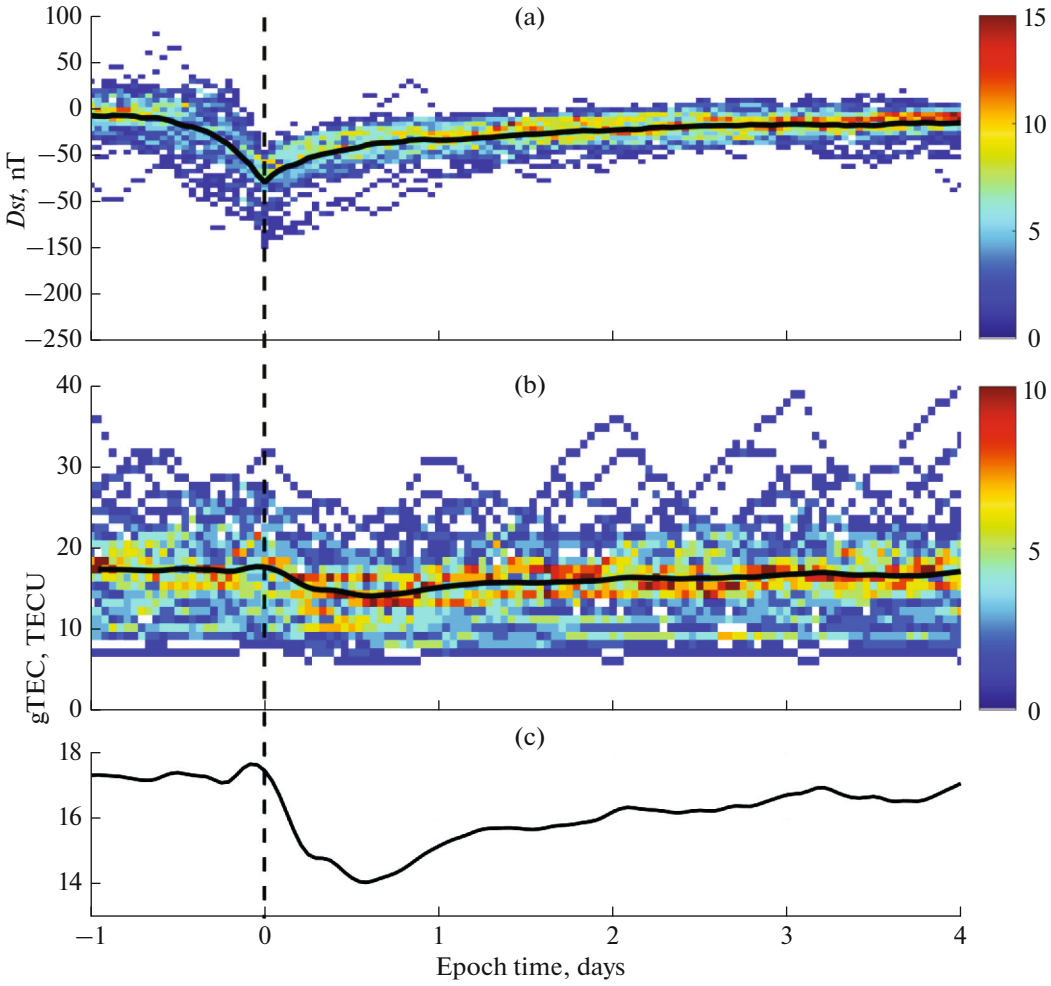

Fig. 6. (a) Dst (b) gTEC, and (c) mean of gTEC for 59 storms in ascending period with peak $Dst \leq -50$ nT as a function of the superposed epoch timeline. The dashed black vertical line show superposed peak *Dst*. The solid black lines provide the mean. The color describes the density of superposed data in 5 nT and 1 TECU by 1-h bins.

age vTEC values showed that there is no significant difference in QD and DD for the high and middle latitudes. In the low latitudes, average vTEC values increased by 50% and 25% in DDs of ascending/descending periods, respectively. Both ascending/descending periods, vTEC values in the low latitudes were found to be 33 and 50% higher than the middle latitudes and 100 and 200% higher than the high latitudes in QD and DD, respectively.

The average values of diurnal vTEC variation for three sectors in QD and DD were obtained for longitudinal analysis. vTEC values in the ascending period are relatively higher than the descending period in both the QD and DD for all sectors. vTECs increased by ~31% in the ascending period and ~33% in the descending period during the DD relative to the QD. Also, the vTEC values of the American sector are relatively higher than the Europe-Africa and Asia-Australia sectors.

The superposed epoch analysis was applied to reveal the characteristic behavior of Dst and gTEC variations during 126 magnetic storms. The peak Dst_{min} values of the storms were superposed. The gTEC values were calculated by average vTECs of CODE-GIM grids, which define global TEC variation. As a remarkable result, the density and mean values of gTEC have a similar pattern, like ordinary *Dst* variation during a magnetic storm. The mean gTEC values have a sudden decrease after the superposed timeline. The decreases were ~20% and ~17% in ascending/descending periods, respectively.

In this study, a comprehensive statistical analysis of global and some local TEC variations was evaluated for magnetically quiet/disturbed periods of the 24th solar cycle. The statistical analysis for different space weather conditions provides crucial data for empirical ionospheric models such as Klobuchar, International Reference Ionosphere (IRI), NeQuick, etc. In future studies, it could be useful to examine the local TEC

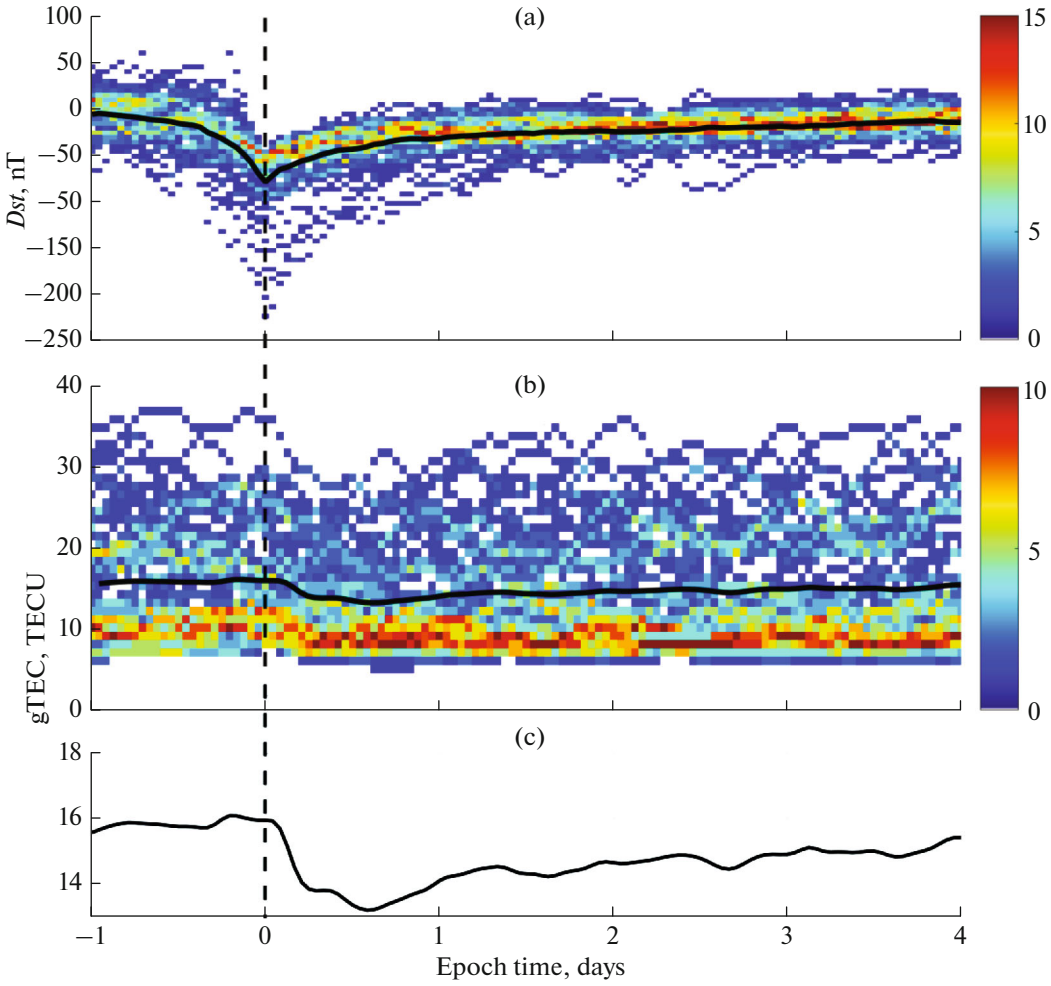

Fig. 7. (a) *Dst* (b) gTEC, and (c) mean of gTEC for 67 storms in descending period with peak $Dst \leq -50$ nT as a function of the superposed epoch timeline. The dashed black vertical line show superposed peak *Dst*. The solid black lines provide the mean. The color describes the density of superposed data in 5 nT and 1 TECU by 1-h bins.

variations during multiple storms with a long term period, such as the one carried out in this study.

REFERENCES

Batista, I.S., De Paula, E.R., Abdu, M.A., Trivedi, N.B., and Greenspan, M.E., Ionospheric effects of the March 13, 1989, magnetic storm at low and equatorial latitudes, *J. Geophys. Res.: Space Phys.*, 1991, vol. 96, no. 8, pp. 13943–13952. 1991.

Bauske, R. and Prölss, G.W., Modeling the ionospheric response to traveling atmospheric disturbances, *J. Geophys. Res.: Space Phys.*, 1997, vol. 102, no. 7, pp. 14555–14562.

Blanc, M. and Richmond, A.D., The ionospheric disturbance dynamo, *J. Geophys. Res.: Space Phys.*, 1980, vol. 85, no. 4, pp. 1669–1686.

Buonsanto, M.J., Ionospheric storms—A review, *Space Sci. Rev.*, 1999, vol. 88, nos. 3–4, pp. 563–601.

Danilov, A.D., Ionospheric *F*-region response to geomagnetic disturbances, *Adv. Space Res.*, 2013, vol. 52, no. 3, pp. 343–366.

Danilov, A.D. and Konstantinova, A.V., Behavior of the ionospheric *F* region prior to geomagnetic storms, *Adv. Space Res.*, 2019, vol. 64, no. 7, pp. 1375–1387.

Davis, C.J., Wild, M.N., Lockwood, M., and Tulunay, Y.K., Ionospheric and geomagnetic responses to changes in IMF Bz: A superposed epoch study, *Ann. Geophys.*, 1997, vol. 15, no. 2, pp. 217–230.

De Abreu, A.J., Martin, I.M., Fagundes, P.R., Venkatesh, K., Batista, I.S., de Jesus, R., Rockenback, M., Coster, A.J., Gende, M., Alves, M.A., and Wild, M., Ionospheric *F* region observations over American sector during an intense space weather event using multi-instruments. *J. Atmos. Sol.-Terr. Phys.*, 2017, vol. 156, pp. 1–14.

Ding, F., Wan, W., Ning, B., and Wang, M., Large-scale traveling ionospheric disturbances observed by GPS total electron content during the magnetic storm of 29–30 October 2003, *J. Geophys. Res.: Space Phys.*, 2007, vol. 112, no. 6, art. ID A06309.

Dmitriev, A.V., Huang, C.M., Brahmanandam, P.S., Chang, L.C., Chen, K.T., and Tsai, L.C., Longitudinal variations of positive dayside ionospheric storms related to recurrent geomagnetic storms, *J. Geophys. Res.: Space Phys.*, 2013, vol. 118, no. 10, pp. 6806–6822.

Gonzalez, W., Guarnieri, F., and Yumoto, K., Global dayside ionospheric response to interplanetary electric fields: Plasma uplift and increases in total electron content, in *Multiscale Coupling of Sun–Earth Processes*, Amsterdam: Elsevier, 2005, pp. 157–171.

Grigorenko, E.I., Lysenko, V.N., Pazyura, S.A., Taran, V.I., and Chernogor, L.F., Ionospheric disturbances during the severe magnetic storm of November 7–10, 2004, *Geomagn. Aeron. (Engl. Transl.)*, 2007, vol. 47, no. 6, pp. 720–738.

Habarulema, J.B., McKinnell, L.A., Burešová, D., Zhang, Y., Seemala, G., Ngwira, C., Chum, J., and Opperman, B., A comparative study of TEC response for the African equatorial and mid-latitudes during storm conditions, *J. Atmos. Sol-Terr. Phys.*, 2013, vol. 102, pp. 105–114.

Ilie, R., Liemohn, M.W., Thomsen, M.F., Borovsky, J.E., and Zhang, J., Influence of epoch time selection on the results of superposed epoch analysis using ACE and MPA data, *J. Geophys. Res.: Space Phys.*, 2008, vol. 113, no. A3.

Inyurt, S., Investigation of ionospheric variations during magnetic storm over Turkey, *Geomagn. Aeron. (Engl. Transl.)*, 2020, vol. 60, no. 1, pp. 131–135.

Katamzi, Z.T. and Habarulema, J.B., Traveling ionospheric disturbances observed at South African midlatitudes during the 29–31 October 2003 geomagnetically disturbed period, *Adv. Space Res.*, 2014, vol. 53, no. 1, pp. 48–62.

Katus, R.M., Liemohn, M.W., Ionides, E.L., Ilie, R., Welling, D., and Sarno-Smith, L.K., Statistical analysis of the geomagnetic response to different solar wind drivers and the dependence on storm intensity, *J. Geophys. Res.: Space Phys.*, 2015, vol. 120, no. 1, pp. 310–327.

Khegai, V.V., Legen'ka, A.D., and Kim, V.P., Comparative analysis of disturbances in the midlatitude ionospheric F2 layer during strong and extreme magnetic storms in March 2001 according to the data from magnetically conjugate ground ionospheric stations, *Geomagn. Aeron. (Engl. Transl.)*, 2009, vol. 49, no. 5, pp. 599–609.

Kumar, S., Sharma, S., and Chandra, H., Interplanetary origin of magnetic storms and their F2-region responses at the equatorial anomaly, *Adv. Space Res.*, 2006, vol. 37, no. 9, pp. 1777–1783.

Liu, W.L., Fu, S.Y., Zong, Q.G., Pu, Z.Y., Yang, J., and Ruan, P., Variations of N^+/O^+ in the ring current during magnetic storms, *Geophys. Res. Lett.*, 2005, vol. 32, no. 15.

Matamba, T.M., Habarulema, J.B., and McKinnell, L.A., Statistical analysis of the ionospheric response during geomagnetic storm conditions over South Africa using ionosonde and GPS data, *Space Weather*, 2015, vol. 13, no. 9, pp. 536–547.

Patel, K., Singh, A., Singh, S.B., and Singh, A.K., Causes responsible for intense and severe storms during the declining phase of Solar Cycle 24, *J. Astrophys. Astron.*, 2019, vol. 40, no. 1, id 4.

Prölss, G.W., Ionospheric F-region storms, in *Handbook of Atmospheric Electrodynamics*, 1995, Volland, H., Ed., Boca Raton: CRC, 1995, pp. 195–248.

Rees, D., Observations and modelling of ionospheric and thermospheric disturbances during major geomagnetic storms: A review, *J. Atmos. Terr. Phys.*, 1995, vol. 57, no. 12, pp. 1433–1457.

Şentürk, E., Investigation of global ionospheric response of the severe geomagnetic storm on June 22–23, 2015 by GNSS-based TEC observations, *Astrophys. Space Sci.*, 2020, vol. 365, id 110. https://doi.org/10.1007/s10509-020-03828-z.

Taylor, J.R., Lester, M., and Yeoman, T.K., A superposed epoch analysis of geomagnetic storms, *Ann. Geophys.*, 1994, vol. 12, no. 7, pp. 612–624.

Timoçin, E. The effect of different phases of severe geomagnetic storms on the low latitude ionospheric critical frequencies, *Adv. Space Res.*, 2019, vol. 64, no. 11, pp. 2280–2289.

Yang, N., Le, H., and Liu, L., Statistical analysis of the mid-latitude trough position during different categories of magnetic storms and different storm intensities, *Earth, Planets Space*, 2016, vol. 68, no. 1, id 171.

Yin, Z., Zou, H., Ye, Y., Zong, Q., and Wang, Y., Superposed epoch analysis of the energetic electron flux variations during CIRs measured by BD-IES, *Space Weather*, 2019, vol. 17, no. 12, pp. 1765–1782.